NIH Public Access
Author Manuscript
J Phys Chem A. Author manuscript; available in PMC 2013 August 13.

Published in final edited form as:
J Phys Chem A. 2007 October 25; 111(42): 10849–10860. doi:10.1021/jp073197r.

Experimental and DFT Studies: Novel Structural Modifications Greatly Enhance the Solvent Sensitivity of Live Cell Imaging Dyes

Alexei Toutchkine[1,2], **Wen-Ge Han**[3,2], **Matthias Ullmann**[4], **Tiqing Liu**[5], **Donald Bashford**[6], **Louis Noodleman**[3,*], and **Klaus M. Hahn**[1,*]

[1]Department of Pharmacology and Lineberger Cancer Center, University of North Carolina at Chapel Hill, Chapel Hill, North Carolina 27599, USA

[3]Department of Molecular Biology, TPC-15, The Scripps Research Institute, 10550 North Torrey Pines Road, La Jolla, California 92037, USA

[4]Structural Biology, University of Bayreuth, Universitätsstr. 30, BGI, 95447 Bayreuth, Germany

[5]University of Maryland Biotechnology Institute, Center for Advanced Research in Biotechnology, 9600 Gudelsky Dr., Rockville, MD 20850, USA

[6]Hartwell Center, St. Jude Children's Research Hospital, 332 N. Lauderdale St. Memphis, TN 38105, USA

Abstract

Structural modifications of previously reported merocyanine dyes (*J. Am. Chem. Soc.* **2003,** *125*, 4132–4145) were found to greatly enhance the solvent dependence of their absorbance and fluorescence emission maxima. Density functional theory (DFT) calculations have been performed to understand the differences in optical properties between the new and previously synthesized dyes. Absorption and emission energies were calculated for several new dyes using DFT vertical self-consistent reaction field methods (VSCRF). Geometries of ground and excited states were optimized with a Conductor-like screening model (COSMO) and self-consistent-field (SCF) methods. The new dyes have enhanced zwitterionic character in the ground state, and much lower polarity in the excited state, as shown by the DFT-VSCRF calculations. Consistently, the position of the absorption bands are strongly blue-shifted in more polar solvent (methanol compared to benzene) as predicted by the DFT spectral calculations. Inclusion of explicit H-bonding solvent molecules within the quantum model further enhances the predicted shifts, and is consistent with the observed spectral broadening. Smaller, but significant spectral shifts in polar versus nonpolar solvent are predicted and observed for emission bands. The new dyes show large fluorescence quantum yields in polar hydrogen bonding solvents; qualitatively, the longest bonds along the conjugated chain at the excited S_1 state minimum are shorter in the more polar solvent, inhibiting photoisomerization. The loss of photostability of the dyes is a consequence of the reaction with and electron transfer to singlet oxygen, starting oxidative dye cleavage. The calculated vertical ionization potentials of three dyes I-SO, AI-SO(4), and AI-BA(4) in benzene and methanol are consistent with their relative photobleaching rates; the charge distributions along the conjugated chains for the three dyes are similarly predictive of higher reaction rates for AI-SO(4) and AI-

[*]Corresponding authors. khahn@med.unc.edu, lou@scripps.edu.
[2]These authors contributed equally to this work.

Supporting Information

The Cartesian coordinates of the S_0 and S_1 state COSMO optimized dye structures, and more detailed atomic ESP charges of the S_0 state dye molecules in MeOH are given in the Supporting Information.

NIH-PA Author Manuscript
NIH-PA Author Manuscript
NIH-PA Author Manuscript

NIH-PA Author Manuscript

NIH-PA Author Manuscript

NIH-PA Author Manuscript

BA(4) than for I-SO. Time dependent DFT (TDDFT) calculations were also performed on AI-BA(4); these were less accurate than the VSCRF method in predicting the absorption energy shift from benzene (C_6H_6) to methanol (MeOH).

1. Introduction

Fluorescent biosensors have enabled visualization of signaling activity in individual, living cells, leading to important insights into spatio-temporal control of signaling pathways.[1–4] Biosensors of protein conformational change have been produced by covalently labeling proteins with solvent-sensitive fluorescent dyes,[5–13] such that protein conformational changes affect fluorescence intensity. We have described such dyes (I-SO, I-TBA, S-SO, and S-TBA)[14] optimized for use in live cell biosensors, with long-wavelength absorbance and emission, high extinction coefficient and quantum yield, water solubility, photostability, and solvent sensitive fluorescence. A novel biosensor of Cdc42 activation made with one of these dyes showed a 3-fold increase in fluorescence intensity in response to GTP-binding by Cdc42.[14]

Using dyes which respond to protein activity by changing fluorescence intensity presents difficulties during imaging, since the fluorescence intensity of dyes depends not only on protein conformational changes, but also on variations in cell thickness, uneven illumination, biosensor concentration etc. In the past, such problems have been overcome by normalizing the biosensor signal against other, non responsive fluorophores which distribute similarly to the biosensor in cells[15]. This presents significant problems that are obstacles to quantitative studies of signaling networks; i.e. the two fluorophores bleach at different rates and site-specific attachment of two fluorophores to a biosensor can be very challenging. Use of a second fluorophore for normalization is not necessary if the dye undergoes a solvent-dependent shift in its excitation or emission maxima, rather than simply an intensity change. Normalization can then be achieved by monitoring the fluorescence intensity of a single dye at two different wavelengths, rather than the relative intensities of two different dyes (see Figure 1).

Our previously reported dyes do possess moderate solvent-dependent shifts in excitation and/or emission wavelengths, but these were insufficient for ratio imaging in cells. The absorption and emission bands present red shifts for I-SO and blue shifts for S-TBA, with increasing solvent polarity. From benzene (C_6H_6) to methanol (MeOH), the absorption and emission wavelength shifts are 15 nm and 12 nm for I-SO, and are 17 nm and 11 nm for S-TBA, respectively. The shifts of the absorption and emission bands of S-SO and I-TBA in other solvents are even smaller.[14] Here we describe structural modifications that enhance the solvent-dependent shifts of excitation/emission wavelengths for these merocyanine dyes. As described by Marder and others,[16–18] merocyanine dyes are insensitive to solvent polarity when their ground states are at the “cyanine limit” (C in Figure 2), with equal contributions from the non-polar and the zwitterionic resonance structures. Dyes at the cyanine limit are characterized by equal dipole moments in the ground and excited states, so solvents affect both states similarly and there is minimal solvent-dependent change in absorption/emission maxima. We expected that by increasing the strength of the electron donor in the dye structure, the dye’s ground state structure would shift to a more polar form (D in Figure 2), and the dye would have greater solvent-dependent absorption/emission wavelengths. This increase in donor strength was accomplished by a novel introduction of a six membered ring into the dye structure. This led to additional aromaticity when the dyes adopted the zwitterionic configuration.

New merocyanine dyes were obtained by adding the 6-membered ring to the electron donating side of previously reported merocyanine structures (Chart 1). All the dyes are

NIH-PA Author Manuscript

NIH-PA Author Manuscript

NIH-PA Author Manuscript

named for the combination of donor and acceptor heterocycles that make up their structure (donors: I = indolenine, S = benzothiazole, O = benzoxazole; acceptors: SO = benzothiophen-3-one-1,1-dioxide, TBA = thiobarbituric acid). In the new dyes an "A" is included in the name of the donor ring structure to denote the enhanced aromaticity imparted by the new six-membered ring (i.e. AI-SO and AI-TBA rather than the previously reported I-SO and I-TBA). The number in parentheses indicates the number of methines in the central polymethine chain.

We will show that the absorption band positions of AI-SO(4), AI-TBA(4), and AI-BA(4) are highly solvent dependent. The shifts of the emission bands of AI-SO(4) and AI-BA(4), though not as significant as the absorption bands, are also largely increased. These two dyes are also highly fluorescent in polar solvents like methanol (MeOH).

In this paper we describe density functional theory (DFT) studies to examine how modifications of the donor structure affect dye solvent sensitivity. Several photophysical properties of these dyes were correctly predicted and analyzed using the DFT vertical self-consistent reaction field (VSCRF)[19,20] method for calculating the spectra, plus a conductor like screening (COSMO)[21–24] solvation model for optimizing geometries. This work points to structural features which can be incorporated to enhance the solvent sensitivity of a broad range of merocyanine dyes.

2. Methods

2.1. Synthesis

The synthesis of the new dyes **1a,b** and **2a–d** was accomplished according to Scheme 1. A detailed description of new synthetic procedures for this family of dyes will be published elsewhere. The synthesis of dyes 3 and 4 (**I-TBA** and **I-SO**) was described previously.[14]

2.2. Computation

All quantum mechanical DFT calculations were performed using the Amsterdam Density Functional (ADF, Version 2000) package.[25] The parametrization of Vosko, Wilk and Nusair (VWN)[26] was used for the local density approximation term, and the corrections of Becke (1988) (B)[27] and Perdew (1986) (P)[28,29] were used for the non-local exchange and correlation terms. The molecular orbitals were expanded in an uncontracted triple-ζ Slater-type orbital basis set, along with a single set of polarization functions. The inner core shells of C(1s), N(1s), O(1s) and S(1s,2p) were treated by the frozen core approximation. The accuracy parameter (accint) for the numerical integration grid was set to 4.0.

We recently established a density functional vertical self-consistent reaction field (VSCRF) solvation model for predicting vertical excitation energies and the solvatochromic shift of solvent sensitive dyes in different solutions.[19] We have successfully applied this method to predict the UV absorption and emission blue shifts of Brooker's merocyanine from $CHCl_3$ to H_2O solutions with increasing solvent polarity, and the solvatochromic shifts of both the absorption and emission processes for S-TBA merocyanine,[30] Abdel-Halim's merocyanine,[31] the rigidified aminocoumarin C153,[32–34] and Nile red,[35,36] in different solutions.[19,20] This VSCRF model was developed in the framework of DFT with ΔSCF methodology. Its implementation is based on our original self-consistent reaction field (SCRF) development,[37–39] where the solute molecule is computed by DFT method in the presence of a solvent reaction field. The reaction field is evaluated from a finite-difference solution to the Poisson-Boltzmann equation and self-consistency between the reaction field and the electronic structure of the solute is achieved by iteration. The SCRF calculation applied to a solute geometry allows the electronic structure relaxation in both the solute and the solvent and, implicitly, the orientational (geometry) relaxation of the solvent. Once the

NIH-PA Author Manuscript

NIH-PA Author Manuscript

NIH-PA Author Manuscript

SCRF calculation on the ground state (S_0) state (or the first excited singlet state (S_1) is achieved, the VSCRF procedure on the excited state (or the ground state) allows only the electronic structure reorganization for both the solute and solvent, and the vertical excitation (or emission) in solution is then obtained. The detailed principles and procedures for VSCRF calculations in both absorption and emission processes, including the ΔSCF spin-decontamination methodology for the first excited singlet state (S_1) energy, can be found in Refs. 19 and 20.

The solute geometries in C_6H_6 and MeOH were optimized using the COSMO (Conductor like Screening Model) model in ADF.[21–24] The COSMO model is a dielectric solvent continuum model in which the solute molecule is embedded in a molecular-shaped cavity surrounded by a dielectric medium with given dielectric constant ε. In our current COSMO and SCRF calculations, we used ε = 2.3 for C_6H_6 and ε = 32.6 for MeOH. The optical dielectric constant ε_{op} = 2 was used in VSCRF calculations. The dielectric boundary between the interior (with ε = 1) and the exterior of the solute region in all COSMO, SCRF and VSCRF calculations was defined by the constant surface of rolling a probe sphere (with radius r = 3.5 and 2.5 Å for C_6H_6 and MeOH, respectively) over the solute. The van der Waals radii for atoms C, O, N, S, and H were taken as 1.7, 1.4, 1.55, 1.8, and 1.2 Å, respectively. Cavitation/dispersion corrections are not included, but these should be similar for the ground and vertical excited states. For the absorption process, the S_0 state of the solute were relaxed in different solvent dielectrics (C_6H_6 and MeOH). Correspondingly, for the emission process, the geometry optimizations were performed on the S_1 state. An electron was promoted from β-HOMO to β-LUMO during the S_1 state geometry optimizations. Our SCRF/VSCRF calculations are then performed on the COSMO-optimized geometries.

As in our earlier work,[19,20] the absorption and emission energies were calculated as vertical excitations in the framework of the Franck-Condon principle[19,20,40] without explicit including of vibrational effects. We neglect zero-point-energies (ZPEs), vibrational thermal energies, and vibrational entropy contributions to the free energy in the ground state and vertical excited state for absorption (and similarly for emission). These effects will partially subtract out in the excitation energies which are energy differences. Further, in the vertical excited state (for absorption), complex issues arise about proper vibrational ensembles, time scales, and partial thermal equilibrium, involving also the solvent bath. While there can be some overall effect of these corrections on the absolute calculated excitation energies, the effects on solvent-dependent shifts are probably small. In contrast to vibrational effects, both COSMO and SCRF/VSCRF calculations include the electronic polarization of the dye by the solvent; the latter effect is important, as will be shown by the differences in dipole moment in different solvents.

3. Results and Discussions

Experimentally we compared merocyanines with more zwitterionic ground states (dyes **1a**, **1b** and **2a–d** in Chart 1) to merocyanines that should be closer to the cyanine limit (dyes **3** and **4** in Chart 1). The more zwitterionic merocyanines were made by incorporating a strong donor ring, either 4-pyridine or 10H-pyrido[1,2-a]indolenine, in the structures. These rings were predicted to stabilize the polar, zwitterionic form of the dyes in the ground state, because of the enhanced aromaticity of the zwitterionic resonance form (Figure 3).

From a theoretical perspective, we have compared DFT calculations, evaluating geometries, excitation and emission energies, H-bonding effects, molecular orbital and bonding characters, dipole moments, and the atomic charge distributions for dyes I-SO (**4**), I-TBA (**3**), AI-SO(4) (**2a**), AI-BA(4) (**2b**), and AI-TBA(4) (**2c**), in order to examine why the

NIH-PA Author Manuscript

NIH-PA Author Manuscript

NIH-PA Author Manuscript

solvent dependencies in absorption and emission, the fluorescence quantum yield, and photobleaching properties change from I-SO to AI-SO(4), and from I-TBA to AI-BA(4) and AI-TBA(4). These properties are also compared in nonpolar C_6H_6 and in polar MeOH solvents.

3.1. Isomers of the Dye Molecules

Using the COSMO model in ADF2000, we geometry optimized all the possible isomer conformations for the dyes 2a-c, 3, and 4 in C_6H_6 ($\varepsilon = 2.3$) and in MeOH ($\varepsilon = 32.6$). NMR spectra of these dyes were consistent with an all-trans configuration of the central polymethine bridge. Our calculations show that the relative energies of the different isomers for each dye are very small (overall < 2.5 kcal mol^{-1}, see Table 1). From an energetic point of view, different isomers for a certain dye may coexist in the solvents. In reality, which isomers that are measured in the experiment highly depend also on the synthetic procedure. Here we simply choose the lowest energy structures of each dye in MeOH for our further calculations in both C_6H_6 and MeOH. These structures with numbering conventions are shown in Chart 2. In fact, our tests using SCRF/VSCRF calculations show very similar electronic structures and absorption energies (with differences normally less than 0.02 eV) for different isomers of a given dye in a given solvent.

3.2. Absorption Spectra

The experimental absorption data for the dyes are summarized in Table 2, and Figure 4. With decreasing solvent polarity, the absorption maximum of dyes **1a–b**, **2a–d** shifted to longer wavelengths, and the intensity of the transition increased (Table 1, Figure 4). Such a hypsochromic (blue) shift is similar to that of Brooker's merocyanine (Figure 5), a well known dye with a ground state predominantly in the zwitterionic form.[19]

For the new dyes with stronger donor rings, a decrease in solvent polarity resulted in destabilization of the zwitterionic form and moved the dye ground state towards the "cyanine limit", increasing the contribution from the non-polar form. The calculated central C-C bond lengths of the ground state geometries are presented in Table 3. Obviously the solute structures vary with solvent polarity. Strong bond length alternations (BLA) were found for merocyanines **2a–c** in MeOH, where dyes predominantly exist as zwitterions. The alternations were diminished in benzene indicating a ground state more like the 'cyanine-limit'. For I-TBA and I-SO, the average BLA was small, suggesting that in both solvents the ground states of the dyes are close to the cyanine limit.

The structure changes of the solutes with increasing solvent polarity from C_6H_6 are consistent with the changes of the solute dipole moment (see Table 4). The S_0 state dipole moments (μ_{S0}) are increased moderately by 6.15 and 4.57 D for I-TBA and I-SO, and significantly by 9.70, 8.82, and 8.45 D for AI-TBA(4), AI-BA(4), and AI-SO(4), respectively, from C_6H_6 to MeOH solutions.

The change of the solute dipole moment in different solutions, or upon $S_0 \rightarrow S_1$ transitions, is caused by charge rearrangement or intramolecular charge transfer. We present in Figure 6 the molecular orbital plots for the electron in the HOMO of the S_0 state and the $\pi \rightarrow \pi$ promoted electron in the S_1 state of dye **2b**, AI-BA(4) in C_6H_6 and in MeOH. The contributions of the atomic π orbitals to the HOMO vary with solvent type. In C_6H_6 solution, the electron in the HOMO is mainly localized at C_7(17.2%), C_3(17.0%), C_5(16.3%), N_{18}(6.6%), C_{16}(5.2%), O_{11}(4.6%), C_1(4.2%), O_{10}(3.8%), and C_2(2.5%). In MeOH solution, the localization of the electron in the HOMO is shifted rightward and localized at the atoms of C_3(17.7%), C_7(17.3%), C_5(16.6%), N_{18}(5.3%), O_{11}(5.0%), C_{16}(4.7%), O_{10}(4.2%), C_1(4.2%), C_6(3.4%), and O_{15}(2.4%). Not only the electron in the

NIH-PA Author Manuscript

NIH-PA Author Manuscript

NIH-PA Author Manuscript

HOMO, but also the distribution of other electrons vary with solvent polarity; therefore the dipole moment of S_0 state AI-BA(4) is substantially increased with increasing solvent polarity from C_6H_6 to MeOH. During the $\pi \rightarrow \pi$ transition, the solute dipole moment decreases. The promoted electron in the π orbital moved leftward. In C_6H_6 solution, it is mainly localized at the atoms of C_4(14.1%), C_2(14.0%), C_6(13.6%), C_{19}(9.7%), N_{18}(7.2%), C_{17}(5.4%), C_5(5.1%), C_{23}(3.2%), O_{10}(3.1%), C_{25}(3.1%), C_8(3.1%), and O_{11}(2.9%) for the vertical S_1 state. In MeOH, the contributions change to C_4(14.4%), C_6(13.9%), C_2(13.0%), N_{18}(8.9%), C_{19}(8.7%), C_{17}(5.5%), C_{16}(4.9%), C_3(3.6%), C_{23}(3.1%), C_8(3.0%), C_{25}(2.9%), and C_9(2.7%).

When the solute dipole moment in the excited state is larger than that in the ground state, the excited state is better stabilized in polar solvents relative to the ground state. With increasing solvent polarity, there will be a red shift for the absorption bands. On the other hand, a blue shift with increasing solvent polarity will occur if the solute dipole moment in the ground state is larger than that in the excited state. During the $\pi \rightarrow \pi$ excitation process, the solute dipole moments of AI-TBA(4), AI-BA(4) and AI-SO(4) all decrease in MeOH solution (Table 4). Their absorption bands shift to the blue with increasing solvent polarity from C_6H_6 to MeOH. By contrast, the dipole moment of I-SO increases during the $\pi \rightarrow \pi$ transition, and we observe the red shift of its absorption band from C_6H_6 to MeOH solution.

In Table 4, we also present the SCRF/VSCRF calculated vertical excitation energies of these molecules. The ΔSCF procedure of DFT method normally under-estimates the absolute value of the S_1 state energy, and therefore also the vertical excitation energy.[19,20] However, the directions and approximate magnitudes of the solvatochromic shift are correctly predicted.

Experimentally we observed a very small red shift for I-TBA with increasing solvent polarity from C_6H_6 to OcOH (with ΔE_{abs} = 0.021 eV, or $\Delta\lambda_{max}$ = 6nm). We did predict a slight red shift for this molecule from C_6H_6 to MeOH (with ΔE_{abs} = 0.012 eV). The observed blue shift from OcOH to MeOH solutions ($\Delta\lambda_{max}$ = 7nm) is possibly caused by the explicit interactions (for instance H-bonding interactions) between the solute and solvent molecules.

Recently, solvent continuum models for predicting the vertical electronic transitions have also been established at the time dependent DFT (TDDFT) level.[41–46] Calculations on the $n = \pi^*$ transition energies of diazines performed by Mennucci[42] and Cossi and Barone[44] have shown results which are in very good agreement with the experiments. However, calculations with TDDFT are still not straightforward in the optimization of gemetries on the excited state surfaces. In order to compare the SCRF/VSCRF and the TDDFT methods, we also applied SCRF/VSCRF calculations on the diazines (see Figure 1 of Ref. 19) to predict the blue shifts with increasing solvent polarities from *n*-heptane to water solutions,[19] and compared our results with the TDDFT[44] and the experimental data.[47] We saw that the TDDFT method was better than the ΔSCF calculations in predicting the absolute values of the vertical excitation energies. However, the blue shifts from *n*-heptane to water obtained by SCRF/VSCRF calculations are much closer to those from the experimental data than those from the TDDFT results, especially for pyridazine and pyrimidine.[19] Both SCRF/VSCRF and TDDFT calculations show that consideration of the explicit water H-bonding effects is very important in order to predict the correct blue shifts for diazines from *n*-heptane to water.[19]

According to ADF's manual, it is possible to combine COSMO model with TDDFT calculations. The usually major effects (modified zeroth-order Kohn-Sham (KS) orbitals and orbital energies) are included. However, COSMO should also modify the first-order change

NIH-PA Author Manuscript

NIH-PA Author Manuscript

NIH-PA Author Manuscript

in the KS potential. This effect has not yet been implemented in ADF and may be significant in case of a high value of the dielectric constant. To see if we can use this TDDFT version in our dye calculations in different solvents, we applied the combination of COSMO and TDDFT at the COSMO optimized geometries of S_0 state AI-BA(4). The results are also given in Table 4. As seen before, the absolute values of the excitation energies predicted by TDDFT are much larger than the ΔSCF calculations,[19] and larger than the experimental spectral energies in the current case. The TDDFT calculations yield very similar excitation energies for AI-BA(4) in C_6H_6 and in MeOH. The energy difference is only 0.026 eV, which is much worse than the SCRF/VSCRF's result (0.172 eV) comparing with the experiment (0.247 eV).

3.3. Broadening of dye absorption in alcohols; role of H-bonding

The dyes studied here have very broad absorption bands in polar, hydrogen bonding solvents such as methanol or ethanol (Figure 4). It is known that the width of a band in the absorption spectrum of a chromophore in solution is a result of two effects: homogeneous and inhomogeneous broadening.

Homogeneous broadening is due to the existence of a continuous set of vibrational sublevels in each electronic state. The homogenous broadening become important for dyes with ground state lying far from cyanine limit. This can be understood by considering that a large amount of charge transfer will result in a large displacement of the excited state potential surface along the solvent reorganization coordinate, leading to a larger degree of direct absorption into higher vibronic levels in the excited state.[18] Inhomogeneous broadening results from the fluctuation of the structure of the solvation shell surrounding the solute. In MeOH solution, there will be more explicit interactions between the solute and the surrounding solvent molecules through H-bonding. Different patterns and numbers of H-bonding interactions may result in a distribution of solute-solvent configurations. The consequent variation in the local electric field leads to a statistical distribution of energies of the electronic transitions. Also, upon excitation, different solute structures and energies may result from the $v = 0$ vibrational level to $v = n$ transitions in the S_1 state. Therefore, the broad absorption bands in MeOH solution result from homogeneous and inhomogeneous effects. According to our isomer geometry and energy calculations given in section 3.1, different isomers of a certain dye may coexist in a certain solvent. In polar solvents like MeOH, different isomers will have different H-bonding interactions with the solvent molecules, which is also a source for the inhomogeneous broadening.

To see how explicit H-bonding and how different numbers of H-bonding interactions influence the solute structure and properties, we took AI-BA(4) as an example and put one, two and three explicit CH_3OH molecules H-bonding to the solute in different positions (Figure 7). The $+1CH_3OH$(I) model contains one CH_3OH molecule at position I, the $+2CH_3OH$(I,II) model has two CH_3OH molecules in total at positions I and II, and the $+3CH_3OH$(I,II,III) model contains all three H-bonding CH_3OH molecules at I, II and III, respectively. The geometries were then optimized using the COSMO model in ADF.

The main bond lengths of these structures are given in Table 5. For comparison, we also include the values for the structure without explicit H-bonding partners. Clearly, the geometry of AI-BA(4) changes upon interaction with the solvent molecule, and also changes with increasing numbers of the H-bonding solvent molecules. First, we look at the central C–C bonds. Without including explicit H-bonding interactions, the C_2–C_3, C_3–C_4, C_4–C_5, C_5–C_6, and C_6–C_7 bond lengths are 1.427, 1.393, 1.416, 1.387, and 1.421 Å, respectively, with obvious single, double, single, double, and single bond characters, consistent with Chart 1. By including one and two H-bonding CH_3OH molecules, these bonding characters are strengthened, with C_2–C_3, C_4–C_5, and C_6–C_7 lengthened, and C_3–C_4, and C_5-C_6

NIH-PA Author Manuscript

NIH-PA Author Manuscript

NIH-PA Author Manuscript

shortened. In the +3CH_3OH(I,II,III) model, the bond lengths of C_2–C_3, C_4–C_5, and C_6–C_7 reach the largest values of 1.444, 1.418, and 1.425 Å, and C_3–C_4, and C_5–C_6 are the shortest bonds 1.380 and 1.383 Å, respectively, among the calculated models. By including explicit H-bonding interactions, the bonding characters of C_1–C_{19} and C_{16}–C_{17} are weakend, and those of C_7–C_8 and C_7–C_9 are strengthened.

The SCRF/VSCRF calculated dipole moment values and vertical excitation energies for these models are given in Table 6. We see that the dipole moment of the solute increases with increasing number of H-bonding solvent molecules. Different models in MeOH produce different absorption energies (E_{abs}), and the E_{abs} value increases with increasing numbers of the H-bonding solvent molecules. In reality, the orientation and the number of the H-bonding interactions between the solute and the solvent molecules may vary and be different from our models. However, our calculations here show that the absorption energy of the solute is influenced by the number and patterns of H-bonding interactions. The excitation energy differences we predicted among the different MeOH H-bonding models are not as large as the broadening we observed experimentally. The inhomogeneous broadening includes molecular dynamics effects which we have not taken into account, and homogeneous broadening as well.

We note that our calculations correspond to $S_0(v = 0) \rightarrow S_1$ vertical transitions. Specifically for absorption, these calculations are performed in the optimal ground state geometry, and the excited state is calculated in the same geometry, assuming the Frank-Condon principle. In reality, the $S_0(v = 0) \rightarrow S_1(v = n)$ (n is largely unidentified) transitions from a distribution of solute-solvent configurations will result in a large span of excitation energies, which are further broadened by the distribution of H-bonding solvent molecules.

In Table 6, we also compared the SCRF/VSCRF calculated and observed energy difference of E_{abs}(MeOH) – E_{abs}(C_6H_6), which represents the blue shift of the absorption band of AI-BA(4) with increasing solvent polarity from C_6H_6 to MeOH. The predicted energy shift gets closer to the experimental value each time we add one, two, and three explicit H-bonding CH_3OH molecules into the quantum region. Especially when considering three H-bonding CH_3OH molecules, our predicted energy shift 0.237 eV is in very good agreement with experimental value of 0.247 eV. Again, we see it is important to take into account the possible explicit H-bonding effects in the SCRF/VSCRF calculations, in order to predict the correct order and reasonable relative excitation energies of the solute molecule in different solvents.

For comparison, we also performed the TDDFT plus COSMO single-point energy calculations on these three COSMO optimized AI-BA(4) structures. Results are also given in Table 6. The current TDDFT plus COSMO calculations yield essentially no difference on the +1, +2, and +3CH_3OH models. Having the explicit H-bonding MeOH molecules with the solute, instead of increasing the blue shift from C_6H_6 to MeOH solvent, TDDFT predicted a decrease of the shift (which was already very small (0.026 eV)), making no difference of the absorption energy of AI-BA(4) in C_6H_6 and in MeOH. The current version of the combination of TDDFT and COSMO in ADF, without modifying the first-order change in the KS potential, is therefore not suitable for solvatochromic studies.

3.4. Fluorescence Spectra of the Dyes

The experimental emission data for the dyes are summarized in Table 7. The SCRF/VSCRF predicted emission energies and the solute dipole moments before and after the vertical emission process are given in Table 8. The dipole moments of AI-BA(4) and AI-SO(4) are further decreased on the S_1 surface after geometry relaxation (in MeOH solution), and then increased during the $S_1 \rightarrow S_0$ transition. This is consistent with the blue shifts of the

NIH-PA Author Manuscript

NIH-PA Author Manuscript

NIH-PA Author Manuscript

emission bands of AI-BA(4) and AI-SO(4) with increasing solvent polarity from C_6H_6 to MeOH. By contrast, the dipole moment of I-SO further decreases after S_1 state geometry relaxation, and then decreases significantly during the vertical emission process. This is also in agreement with the red shift of the I-SO emission band with increasing solvent polarity from C_6H_6 to MeOH. Similarly to the absorption case, we predicted a negligible red shift (ΔE_{em} = 0.017 eV) for the emission band of I-TBA with increasing solvent polarity. In reality, there does exist a small red shift from C_6H_6 to DMF (with ΔE_{em} = 0.020 eV, or $\Delta\lambda_{max}$ = 6nm). The nearly equal emission energy observed in C_6H_6 and MeOH may again result in the explicit interactions between the solute and solvent molecules.

For the emission energy of AI-BA(4) in MeOH, the E_{em} values also increase with increasing number of the H-bonding solvent molecules. The increment, however, is much less than the corresponding ones in the absorption process. This may also be explained by the smaller change of the dipole moment μ_{S1} from one model to another, compared with the corresponding change of μ_{S0}. This may also be the reason that the width of the emission band in MeOH is not as broad as the absorption band.

3.5. Fluorescence quantum yield

The fluorescence quantum yield (Φ) is determined by the competition between fluorescence and non-radiatiative pathways. Many factors can affect the fluorescence quantum yield, such as, temperature (which influences the intramolecular vibrations, rotations or isomerizations, and the collisions of the solute and solvent, etc.), pH, polarity, viscosity, hydrogen bonding, presence of quenchers, and formation of new complex.[48]

The main nonfluorescent deactivation path for the excited state of Merocyanine 540 (MC 540), which is closely related to our dyes, is photoisomerization around central double bond.[49–51] It was supposed that partial rotation around the double bond in the excited state of MC 540 will result in formation of a perpendicular transition state that collapses to a highly excited vibronic level of the ground state, with consequent thermal dissipation of energy.[49] Work with structurally similar dyes has established that in a given solvent, the height of the barrier to internal rotation decreases with decreasing bond order of isomerizing bond.[50]

The quantum yield of fluorescence of MC 540 increases with increase in solvent shear viscosity, a trend which is true for dyes **1a–b**, **2a–d**, **3** and **4** (Table 7), suggesting the importance of photoisomerization for our dyes. It has been previously shown that the rate of photoisomerization of MC 540 can be correlated to solvent polarity. For example, in alcohols the photoisomerization rate is higher than in nitriles with similar viscosities.[52] This is partly because the hydrogen bonding alcohols better stabilize the twisted excited state of MC 540, which has a substantial zwitterionic character leading to faster photoisomerization.

Since the explicit solute-solvent interactions vary with the solvents, and so many factors will influence the fluorescence and life times, it is not an easy task to predict or analyze the Φ values in each solvent. Here we will analyze the geometric and electronic structures of the dye molecules in C_6H_6 and in MeOH, in order to have an idea how the fluorescence quantum yield changes in general from non-polar to polar solvents, without considering the explicit solute-solvent interactions. There is a striking difference between fluorescence quantum yields in benzene and methanol for dyes AI-SO(4), AI-BA(4) and I-SO, even though these are solvents with similar viscosities (Table 7). For I-SO, we have $\Phi(C_6H_6)$ = 0.42 > Φ(MeOH) = 0.08. In contrast, for AI-SO(4), $\Phi(C_6H_6)$ = 0.19 < Φ(MeOH) = 0.54. In Table 9, we present the calculated central C-C bond lengths of the relaxed S_1 state for I-SO and AI-SO(4). The molecular orbital plots of the ground state (S_0) HOMO and the S_1 state promoted electron are shown in Figure 8 (for I-SO) and Figure 9 (for AI-SO(4)). For I-SO,

NIH-PA Author Manuscript

NIH-PA Author Manuscript

NIH-PA Author Manuscript

after excitation in C_6H_6, the bond lengths of C_2-C_3, C_4-C_5 and C_6-C_7 are lengthened (see Tables 3 and 9), and these three bonds change from bonding to non-bonding, bonding to anti-bonding, and non-bonding to anti-bonding characters, respectively (see Figure 8). Now r(C_4-C_5) = 1.408 Å becomes the longest in the S_1 state. It is therefore very likely that the main photo-isomerization coordinate is the internal rotation of C_4-C_5 for I-SO in C_6H_6 since this is the weakest bond with the greatest single bond character. In MeOH, after excitation, the bond lengths of C_3-C_4 and C_5-C_6 are lengthened, and their bonding characters are changed from non-bonding to anti-bonding (for C_3-C_4) and bonding to non-bonding (for C_5-C_6). Now r(C_3-C_4) = 1.414 Å, and r(C_5-C_6) = 1.410 Å. Both are longer than r(C_4-C_5) in C_6H_6. Also, the central C-C bonds of the S_1 state of I-SO in MeOH have distinct single or double bond character. By contrast, these bonds show very similar distances in C_6H_6 solution. Therefore, the internal rotations around C_3-C_4 and C_5-C_6 for the S_1 state of I-SO in MeOH will be easier than any bond rotations of the S_1 state of I-SO in C_6H_6. This is probably the reason that the fluorescence quantum yield of I-SO in MeOH is smaller than in C_6H_6.

For the S_1 state AI-SO(4) in C_6H_6, r(C_2-C_3) = 1.430 Å is obviously longer than other central C-C bonds (Table 9), and its bond character changes from bonding to non-bonding upon excitation (Figure 9). For the S_1 state AI-SO(4) in MeOH, though this bond is still the longest (1.420 Å), it has bonding character (Figure 9) and it is shortened upon excitation (Tables 3 and **9**). The other possible rotating bonds are C_3-C_4 and C_5-C_6, which are lengthened after excitation, and their bonding characters change from non-bonding to anti-bonding (for C_3-C_4) and bonding to non-bonding (for C_5-C_6). These two bond lengths r(C_3-C_4) = 1.416 Å and r(C_5-C_6) = 1.414 Å in MeOH are much shorter than r(C_2-C_3) = 1.430 Å in C_6H_6. Therefore, the internal rotation or photo-isomerization for the S_1 state AI-SO(4) around C_2-C_3 in C_6H_6 will be easier than the rotation around C_2-C_3, C_3-C_4 or C_5-C_6 in MeOH, and the fluorescence quantum yield of AI-SO(4) in C_6H_6 is thus lower than that in MeOH. The same reason applies for the lower fluorescence quantum yield of AI-BA(4) in C_6H_6 relative to MeOH (Figure 6).

3.6. Photostability

The photostability of dyes is very important for applications in living cells. We have been studying the mechanism of photobleaching for merocyanines of varying structure.[14] The photostability of the new dyes was characterized by exposing them to constant illumination from a halogen tungsten lamp filtered through glass. This broad spectrum light source provided essentially equal intensity throughout the spectral range where the dyes absorb, and where they would be irradiated *in vivo* (600–650 nm). Bleaching occurred through intermediate formation of singlet oxygen. Photobleaching rates of the new dyes are compared in Table 10.

The bleaching rates for the dyes differed by two orders of magnitude. The relative rate constants k_r (rel) for product formation during reaction with singlet oxygen were measured by comparing the percent conversions for dyes dissolved in DMSO containing a fixed amount of $^1O_2$ (2.5 mM solutions; $^1O_2$ generated by decomposition of 1,4-dimethylnaphtalene-1,4-endoperoxide). The rates were generally higher for dyes with a polar ground state (**1a**, **2a**, **2b**, **2d**) than for the dyes with their ground state at the “cyanine limit” (**3**, **4**). Careful analysis of reaction mixtures revealed that the major product of dye **3** photooxidation was indol-2-one **10**, while the major product of photooxidation of dye **2a** is acetal **11** (Figure 10). The detailed analysis of these reactions and reactions products will be published elsewhere. Olefins without allylic hydrogens react with singlet oxygen to form dioxetanes. Dioxetanes are unstable and decompose, to form two carbonyl compounds.

NIH-PA Author Manuscript

NIH-PA Author Manuscript

NIH-PA Author Manuscript

The mechanism of the reaction can be a concerted [2+2] addition of singlet oxygen or it can be a polar reaction, depending on the olefin structure. Olefins with donor substituents react with singlet oxygen to form dioxetanes via zwitterionic 1,4-dipolar species. Because our dyes have donor substituents (nitrogens) it is likely that the reaction proceeds through a zwitterionic mechanism. (Scheme 2). The incipient reactivity of the dyes will be determined by the extent of negative charge at carbon atom C_3, which is the most negatively charged atom in the dye molecules (Table 11, also see Figure S1 in Supporting Information). One can think of this as a charge-induced dipole interaction between C_3 and $^1O_2$. Our calculation showed that this charge is higher for AI-SO(4) and AI-BA(4), which react faster with singlet oxygen.

It has been suggested that the initial interaction of $^1O_2$ with C=C bonds is a single-atom, end-on interaction.[40] Previous studies show that the initial stage of the reaction generally proceeds through charge transfer (substrate electron donor $^1O_2$ electron acceptor).[40] Therefore the rates of reaction with $^1O_2$ normally increase as the ionization potential of the substrate decreases. We calculated the vertical ionization potentials (ΔE_I) of I-SO, AI-SO(4) and AI-BA(4), and compared them in Table 12. ΔE_I is defined as:

$$\Delta E_I = E^+ - E_0 \quad (1)$$

where E_0 is the full SCRF energy calculated at the COSMO-optimized geometry of the neutral ground state dye molecule in a certain solvent, and E^+ is the VSCRF energy for the dye with a positive charge at the same geometry in the same solvent. Clearly, the calculated ionization potentials of AI-SO(4) and AI-BA(4) are lower than the corresponding value of I-SO in both C_6H_6 and MeOH solutions. It is therefore easier for AI-SO(4) and AI-BA(4) to transfer an electron to $^1O_2$; AI-SO(4) and AI-BA(4) show much higher photobleaching rates (Table 10) than I-SO, as expected based on the calculated ionization potentials. We also see that $\Delta E_I(\text{MeOH}) > \Delta E_I(C_6H_6)$ for each of the dye molecules. This is consistent with the fact that the experimentally observed photobleaching rates of AI-SO(4) and I-SO are higher in C_6H_6 than in MeOH.

4. Conclusion

New merocyanine dyes with an enhanced contribution of the zwitterionic ground state resonance form have been prepared through incorporation of a six membered ring in the electron donor portion of the molecule. Positions of the absorption and emission bands for the new dyes strongly depend on solvent polarity. Their photophysical properties were correctly predicted using the SCRF/VSCRF method plus COSMO solvation model. We found that explicit H-bonding solvent interactions were important to include in calculations to predict the correct order of the excitation and emission energies. In contrast to MC540, the new dyes show large fluorescence quantum yields in polar hydrogen-bonding solvents. This can be explained by the DFT results that charge transfer upon excitation produces an excited state with a low contribution from the zwitterionic form. The non-polar excited state is less susceptible to hydrogen bond formation with solvent and consequent non-radiative activation through photoisomerization.

Since the positions of singlet oxygen attack in the dye molecules are predicted (atom C_3), efforts are being made to improve the photostability of these dyes by attaching an electron-accepting group to atom C_3 to inhibit the charge transfer from C_3 to $^1O_2$. The cyano-group (C≡N) has been chosen for this purpose and attached to I-SO and S-SO.[53] This greatly improved the photostability of the dyes.[53] Efforts to improve the photostability of other solvent-sensitive dyes are ongoing. On the other hand, photobleaching of the new dyes can be useful in making powerful phototoxins. It is well known that certain cyanine dyes, such

NIH-PA Author Manuscript

NIH-PA Author Manuscript

NIH-PA Author Manuscript

as MC540, are selectively assimilated into leukemia cells, even in the presence of a large excess of healthy cells.[49,51,54–56] They can be used to detect labelled cells, and then function as potent phototoxins toward the host cells after photobleaching. MC540, however, suffers from its very modest quantum yields of both triplet formation and singlet molecular oxygen generation. There is scope for an increase in cytotoxicity by improving the photophysical properties without significantly changing molecular properties such as selectivity and cellular/tissue localization.[57]

Supplementary Material

Refer to Web version on PubMed Central for supplementary material.

Acknowledgments

Financial support from the NIH (grants GM057464 and GM064346 for K.H.; and GM43278 for L.N.), Novartis, and Panomics, Inc. is gratefully acknowledged. The support of computer resources of The Scripps Research Institute is also acknowledged.

References

1. Hahn K, Toutchkine A. Curr Opin Cell Biol. 2002; 14:167–172. [PubMed: 11891115]
2. Kraynov VS, Chamberlain C, Bokoch GM, Schwartz MA, Slabaugh S, Hahn KM. Science. 2000; 290:333–337. [PubMed: 11030651]
3. Chamberlain C, Hahn KM. Traffic. 2000; 1:755–762. [PubMed: 11208065]
4. Hahn K, Debiasio R, Taylor DL. Nature. 1992; 359:736–738. [PubMed: 1436037]
5. Giuliano KA, Taylor DL. Trends Biotech. 1998; 16:135–140.
6. Cerione RA. Heterotrimeric G Proteins: Methods Enzymol. 1994; 237:409–423.
7. Nomanbhoy TK, Cerione RA. J Biol Chem. 1996; 271:10004–10009. [PubMed: 8626553]
8. Nomanbhoy T, Cerione RA. Biochem. 1999; 38:15878–15884. [PubMed: 10625453]
9. Baburaj K, Azam N, Udgaonkar D, Durani S. Biochim Biophys Acta Gen Subj. 1994; 1199:253–265.
10. Prendergast FG, Meyer M, Carlson GL, Iida S, Potter JD. J Biol Chem. 1983; 258:7541–7544. [PubMed: 6408077]
11. Rasmussen SGF, Carroll FI, Maresch MJ, Jensen AD, Tate CG, Gether U. J Biol Chem. 2001; 276:4717–4723. [PubMed: 11062247]
12. Morii T, Sugimoto K, Makino K, Otsuka M, Imoto K, Mori Y. J Am Chem Soc. 2002; 124:1138–1139. [PubMed: 11841260]
13. Daugherty DL, Gellman SH. J Am Chem Soc. 1999; 121:4325–4333.
14. Toutchkine A, Kraynov V, Hahn K. J Am Chem Soc. 2003; 125:4132–4145. [PubMed: 12670235]
15. Nalbant P, Hodgson L, Kraynov V, Toutchkine A, Hahn KM. Science. 2004; 305:1615–1619. [PubMed: 15361624]
16. Bourhill G, Bredas JL, Cheng LT, Marder SR, Meyers F, Perry JW, Tiemann BG. J Am Chem Soc. 1994; 116:2619–2620.
17. Gorman CB, Marder SR. Chem Mater. 1995; 7:215–220.
18. Bublitz GU, Ortiz R, Marder SR, Boxer SG. J Am Chem Soc. 1997; 119:3365–3376.
19. Liu T, Han WG, Himo F, Ullmann GM, Bashford D, Toutchkine A, Hahn KM, Noodleman L. J Phys Chem A. 2004; 108:3545–3555.
20. Han WG, Liu T, Himo F, Toutchkine A, Bashford D, Hahn KM, Noodleman L. ChemPhysChem. 2003; 4:1084–1094. [PubMed: 14596006]
21. Klamt A, Schüürmann G. J Chem Soc Perkin Trans II. 1993:799–805.
22. Klamt A. J Phys Chem. 1995; 99:2224–2235.
23. Klamt A, Jonas V. J Chem Phys. 1996; 105:9972–9981.

NIH-PA Author Manuscript

NIH-PA Author Manuscript

NIH-PA Author Manuscript

24. Pye CC, Ziegler T. Theor Chem Acc. 1999; 101:396–408.
25. ADF 2000.02; SCM, Theoretical Chemistry. Vrije Universiteit; Amsterdam, The Netherlands: http://www.scm.com
26. Vosko SH, Wilk L, Nusair M. Can J Phys. 1980; 58:1200–1211.
27. Becke AD. Physical Review A. 1988; 38:3098–3100. [PubMed: 9900728]
28. Perdew JP. Phys Rev B. 1986; 33:8822–8824.
29. Perdew JP. Phys Rev B. 1986; 34:7406–7406.
30. Hahn KM, Waggoner AS, Taylor DL. J Biol Chem. 1990; 265:20335–20345. [PubMed: 2173702]
31. Abdel-Halim ST. J Chem Soc Faraday Trans. 1993; 89:55–57.
32. Jones G, Jackson WR, Choi C, Bergmark WR. J Phys Chem. 1985; 89:294–300.
33. Gustavsson T, Cassara L, Gulbinas V, Gurzadyan G, Mialocq JC, Pommeret S, Sorgius M, van der Meulen P. J Phys Chem A. 1998; 102:4229–4245.
34. Mccarthy PK, Blanchard GJ. J Phys Chem. 1993; 97:12205–12209.
35. Davis MM, Hetzer HB. Anal Chem. 1966; 38:451–461.
36. Sackett DL, Wolff J. Anal Biochem. 1987; 167:228–234. [PubMed: 3442318]
37. Chen JL, Noodleman L, Case DA, Bashford D. J Phy Chem. 1994; 98:11059–11068.
38. Bashford, D. An Object-Oriented Programming Suite for Electrostatic Effects in Biological Molecules. In: Ishikawa, Y.; Oldehoeft, RR.; Reynders, JVW.; Tholburn, M., editors. Scientific Computing in Object-Oriented Parallel Environments (Lecture Notes in Computer Science). Vol. 1343. Springer; Berlin: 1997. p. 233-240.
39. Li J, Nelson MR, Peng CY, Bashford D, Noodleman L. J Phys Chem A. 1998; 102:6311–6324.
40. Turro, NJ. Modern Molecular Photochemistry. University Science Books; Mill Valley: 1991.
41. Mennucci B, Cammi R, Tomasi J. J Chem Phys. 1998; 109:2798–2807.
42. Mennucci B. J Am Chem Soc. 2002; 124:1506–1515. [PubMed: 11841322]
43. Cossi M, Barone V. J Chem Phys. 2000; 112:2427–2435.
44. Cossi M, Barone V. J Chem Phys. 2001; 115:4708–4717.
45. Cossi M, Rega N, Scalmani G, Barone V. J Chem Phys. 2001; 114:5691–5701.
46. Barone V, Palma A, Sanna N. Chemical Physics Letters. 2003; 381:451–457.
47. Baba H, Goodman L, Valenti PC. J Am Chem Soc. 1966; 88:5410–5415.
48. Valeur, B. Molecular Fluorescence: Principles and Applications. WILEY-VCH Verlag GmbH; Weinheim: 2002.
49. Benniston AC, Harriman A, McAvoy C. J Chem Soc, Faraday Trans. 1997; 93:3653–3662.
50. Benniston AC, Harriman A. J Chem Soc, Faraday Trans. 1994; 90:2627–2634.
51. Benniston AC, Harriman A. J Chem Soc, Faraday Trans. 1998; 94:1841–1847.
52. Onganer Y, Yin M, Bessire DR, Quitevis EL. J Phys Chem. 1993; 97:2344–2354.
53. Toutchkine A, Nguyen D-V, Hahn KM. Org Lett. 2007 in press.
54. Singh RJ, Feix JB, Kalyanaraman B. Photochem Photobiol. 1992; 55:483–489. [PubMed: 1620725]
55. Franck B, Schneider U. Photochem Photobiol. 1992; 56:271–276. [PubMed: 1502270]
56. Sieber F. Photochem Photobiol. 1987; 46:1035–1042. [PubMed: 3325998]
57. Redmond RW, Srichai MB, Bilitz JM, Schlomer DD, Krieg M. Photochem Photobiol. 1994; 60:348–355. [PubMed: 7527561]

NIH-PA Author Manuscript

NIH-PA Author Manuscript

NIH-PA Author Manuscript

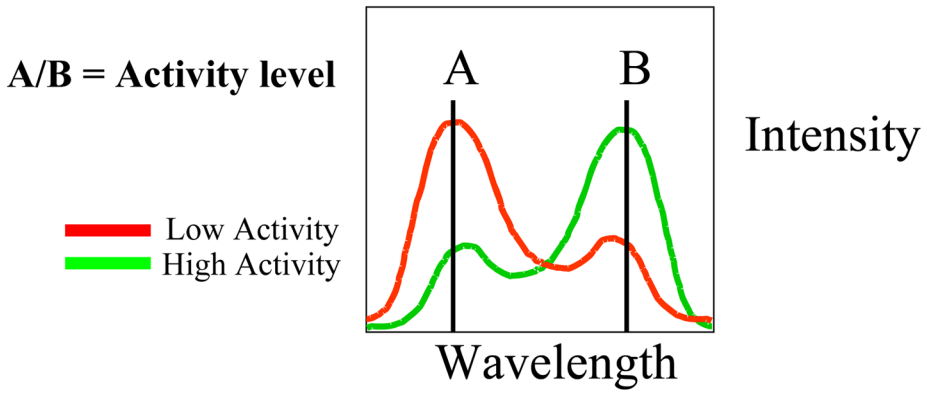

Figure 1.
Ratio imaging. When covalently attached to a protein, the dye molecule shifts between two spectra (i.e. spectrum A and spectrum B), as the dye environment is affected by protein conformational changes. Intensity A divided by intensity B reflects the protein environment, regardless of the overall intensity of the fluorescence.

NIH-PA Author Manuscript

NIH-PA Author Manuscript

NIH-PA Author Manuscript

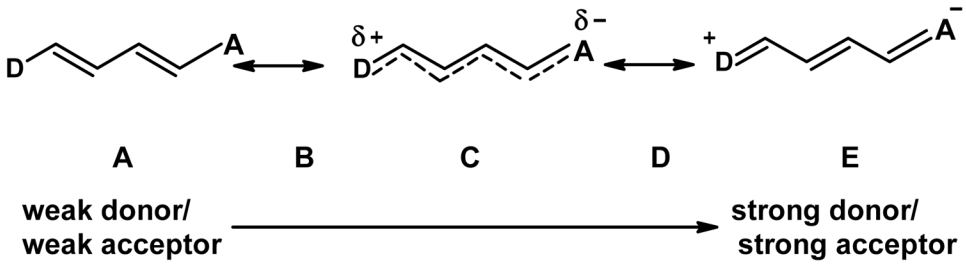

Figure 2.

Resonance structures of merocyanine dyes. Depending on the relative electron donating and accepting strength of the “donor” (D) and “acceptor” (A) portions of the molecule, the dye can adopt different ground state structures, ranging from neutral through zwitterionic.

NIH-PA Author Manuscript

NIH-PA Author Manuscript

NIH-PA Author Manuscript

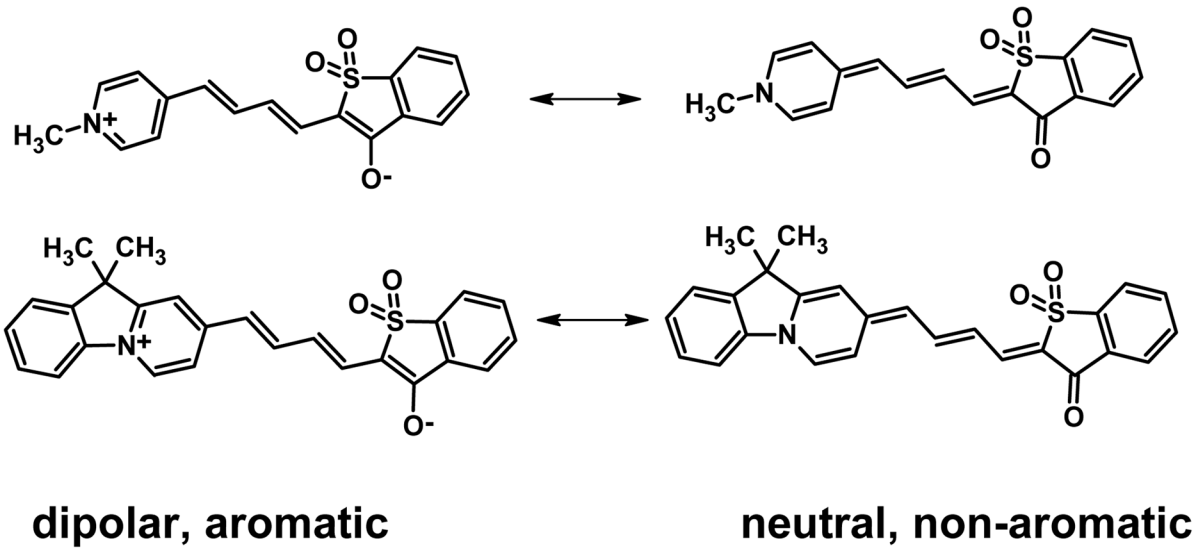

Figure 3.
Ground state of merocyanine dyes with and without aromatic stabilization of a charged donor ring. The incorporation of an additional 6-membered ring strongly favors the charged zwitterionic resonance form.

NIH-PA Author Manuscript

NIH-PA Author Manuscript

NIH-PA Author Manuscript

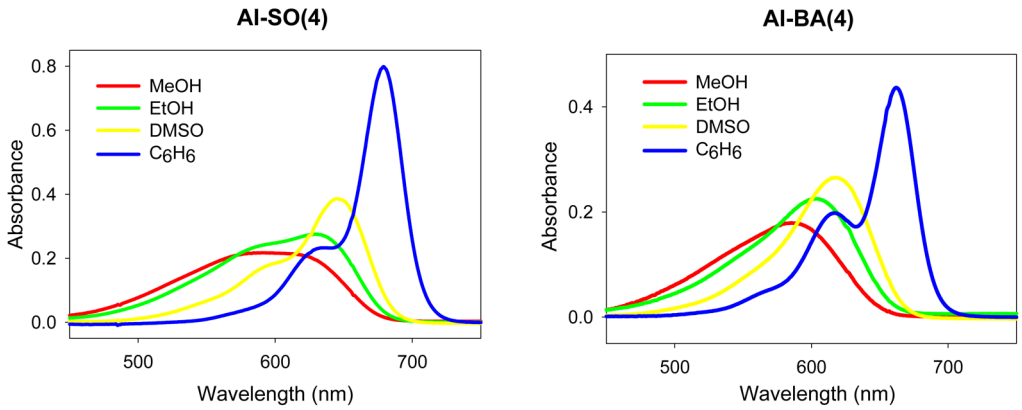

Figure 4.

Absorbance spectra of **AI-BA(4)** and **AI-SO(4)** in methanol, ethanol, DMSO, and benzene. C(**AI-BA(4)**) = 2.17 μM, C(**AI-SO(4)**) = 3.33 μM.

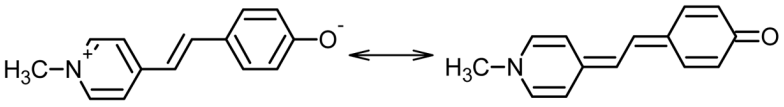

Figure 5.
Brooker's merocyanine.

NIH-PA Author Manuscript
NIH-PA Author Manuscript
NIH-PA Author Manuscript

NIH-PA Author Manuscript

NIH-PA Author Manuscript

NIH-PA Author Manuscript

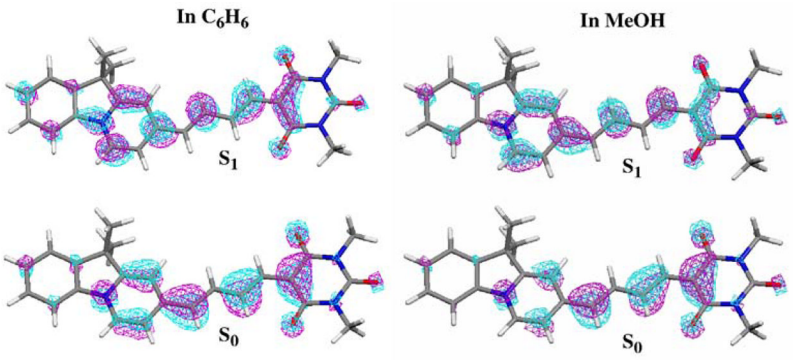

Figure 6.
Molecular orbital plots for the electron in the HOMO of the ground state (S_0) and the $\pi \rightarrow \pi$ promoted electron in the first excited singlet state of AI-BA(4) in C_6H_6 and in MeOH.

NIH-PA Author Manuscript
NIH-PA Author Manuscript
NIH-PA Author Manuscript

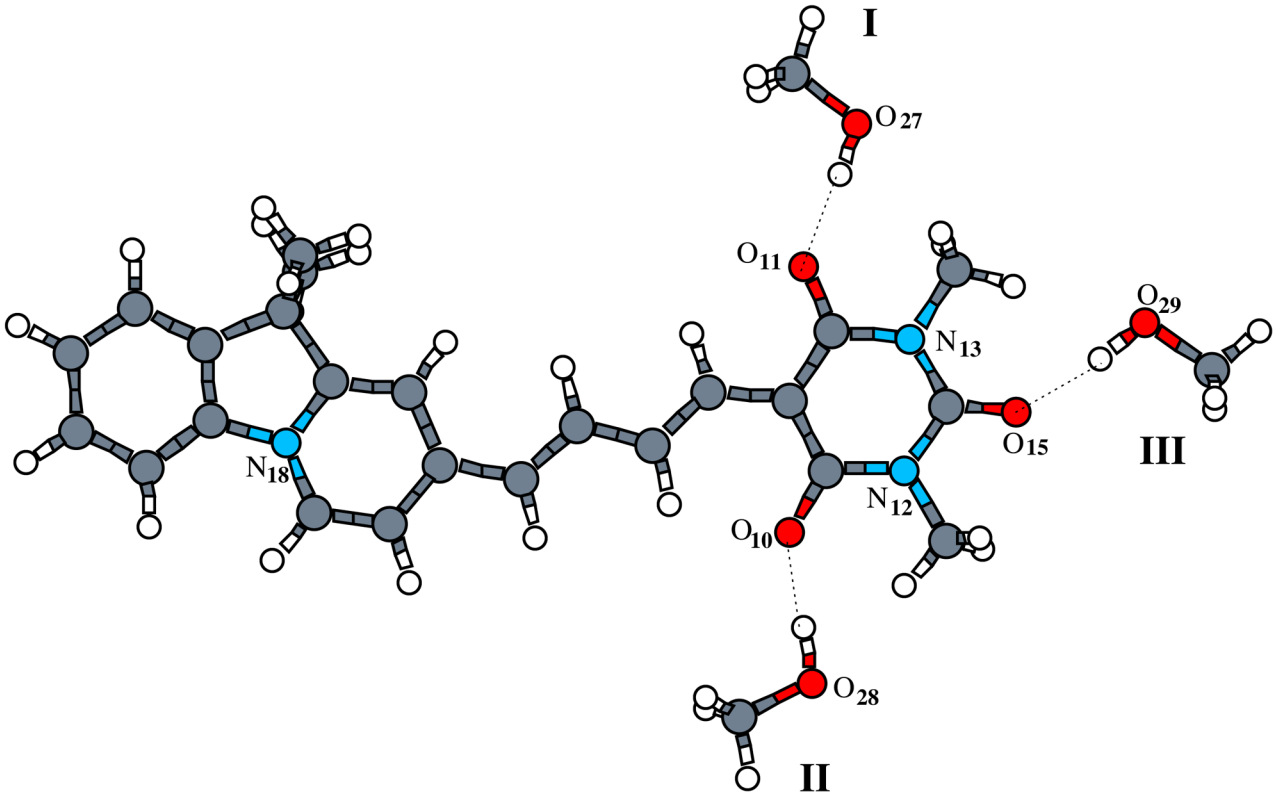

Figure 7.
Three possible positions of the explicit CH_3OH molecules H-bonding to AI-BA(4) in MeOH solution.

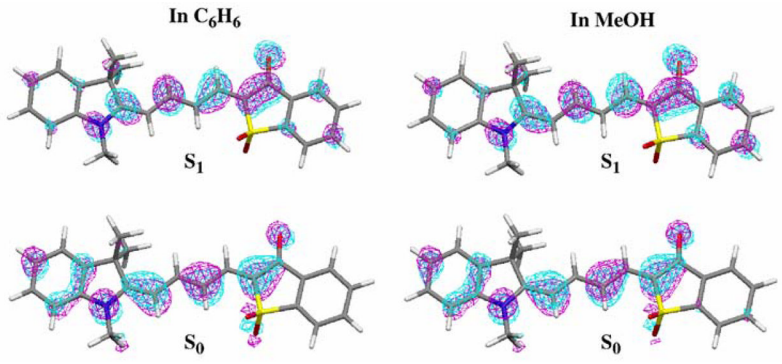

Figure 8.
Molecular orbital plots for the electron in HOMO of the S_0 state and the $\pi \rightarrow \pi$ promoted electron in the S_1 state of I-SO in C_6H_6 and in MeOH.

NIH-PA Author Manuscript
NIH-PA Author Manuscript
NIH-PA Author Manuscript

NIH-PA Author Manuscript

NIH-PA Author Manuscript

NIH-PA Author Manuscript

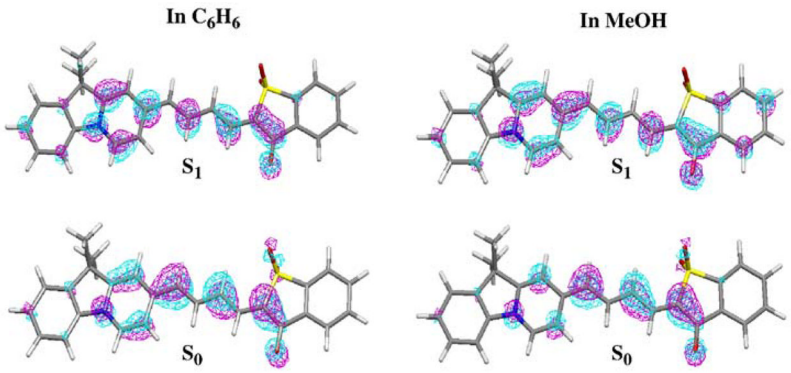

Figure 9.

Molecular orbital plots for the electron in HOMO of the S_0 state and the $\pi \rightarrow \pi$ promoted electron in the S_1 state of AI-SO(4) in C_6H_6 and in MeOH.

NIH-PA Author Manuscript

NIH-PA Author Manuscript

NIH-PA Author Manuscript

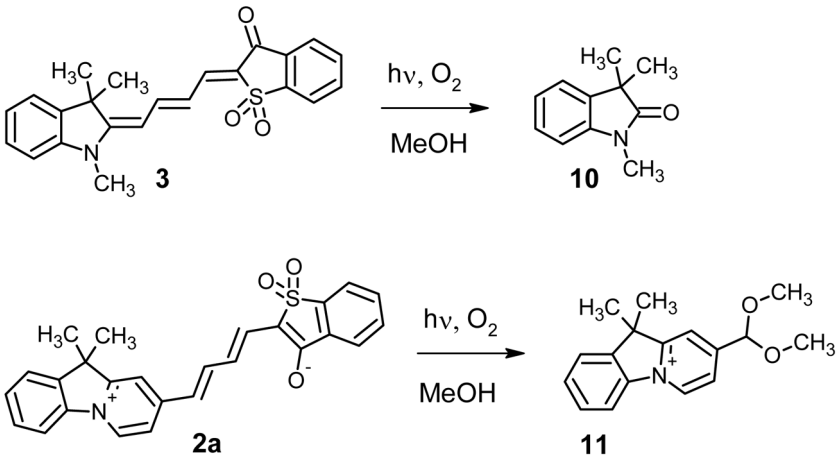

Figure 10.
Products of photobleaching reactions of merocyanine dyes.

NIH-PA Author Manuscript

NIH-PA Author Manuscript

NIH-PA Author Manuscript

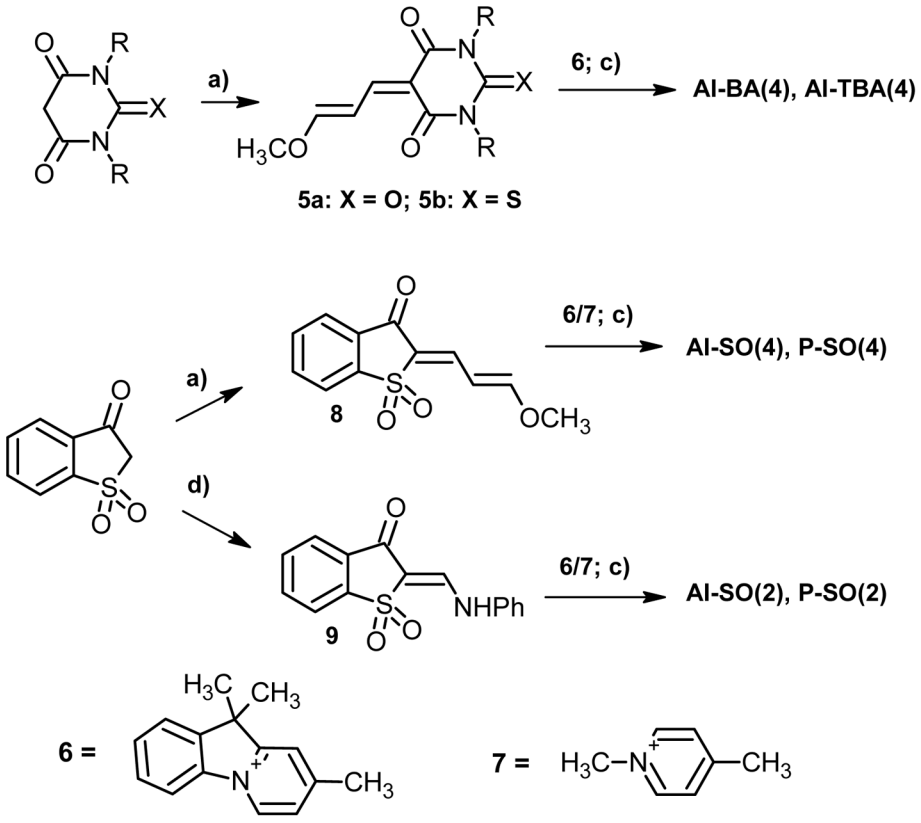

Scheme 1.

Synthesis of dyes **1a, b, 2a-2d.** Conditions: (a) malonoaldehyde bis(dimethyl acetal), CF_3COOH, 95° C, 2 hours. (b) malonoaldehyde bis(dimethyl acetal), CF_3COOH, 130° C, 2 hours. (c) N-Methylpiperidine, MeOH, reflux 30–60 min. (d) diphenylformamidine, AcOH-Ac2O, 120° C, 2 hours.

NIH-PA Author Manuscript

NIH-PA Author Manuscript

NIH-PA Author Manuscript

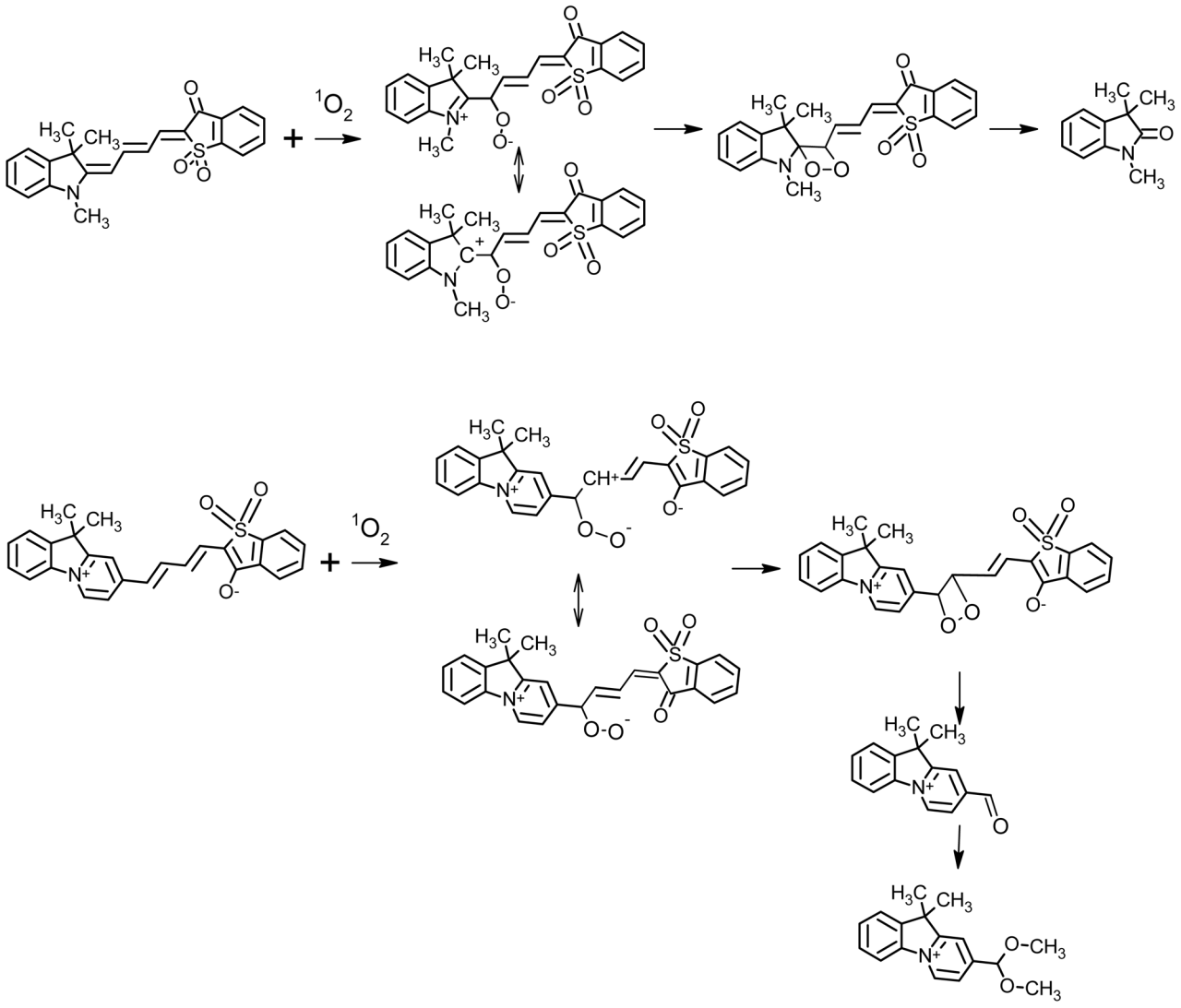

Scheme 2.
Photooxidation of I-SO and AI-SO(4) dyes.

NIH-PA Author Manuscript

NIH-PA Author Manuscript

NIH-PA Author Manuscript

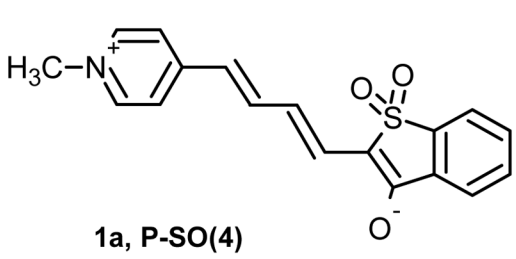

1a, P-SO(4)

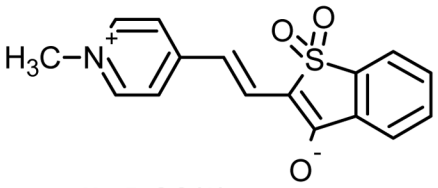

1b, P-SO(2)

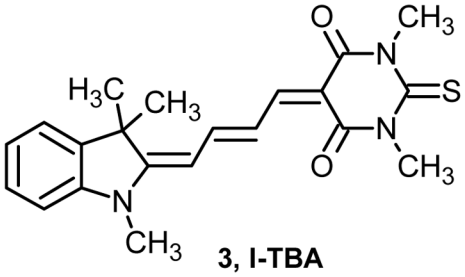

3, I-TBA

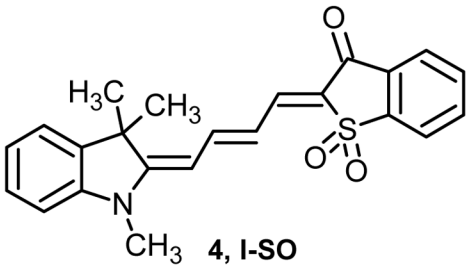

4, I-SO

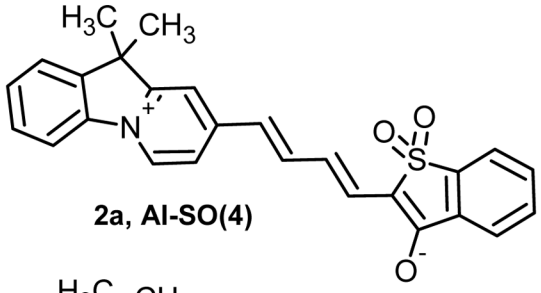

2a, AI-SO(4)

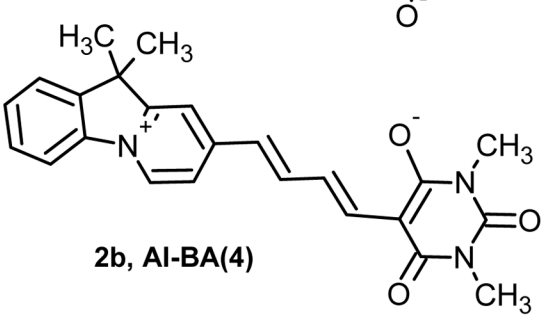

2b, AI-BA(4)

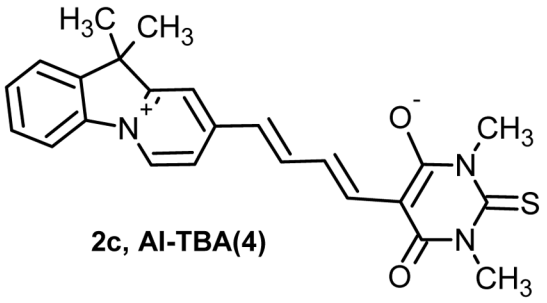

2c, AI-TBA(4)

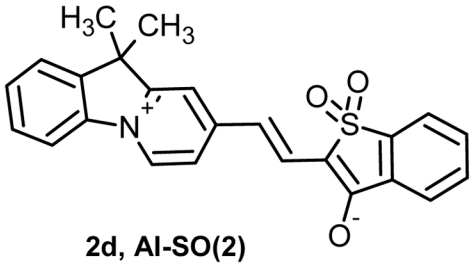

2d, AI-SO(2)

Chart 1.
Dye structures

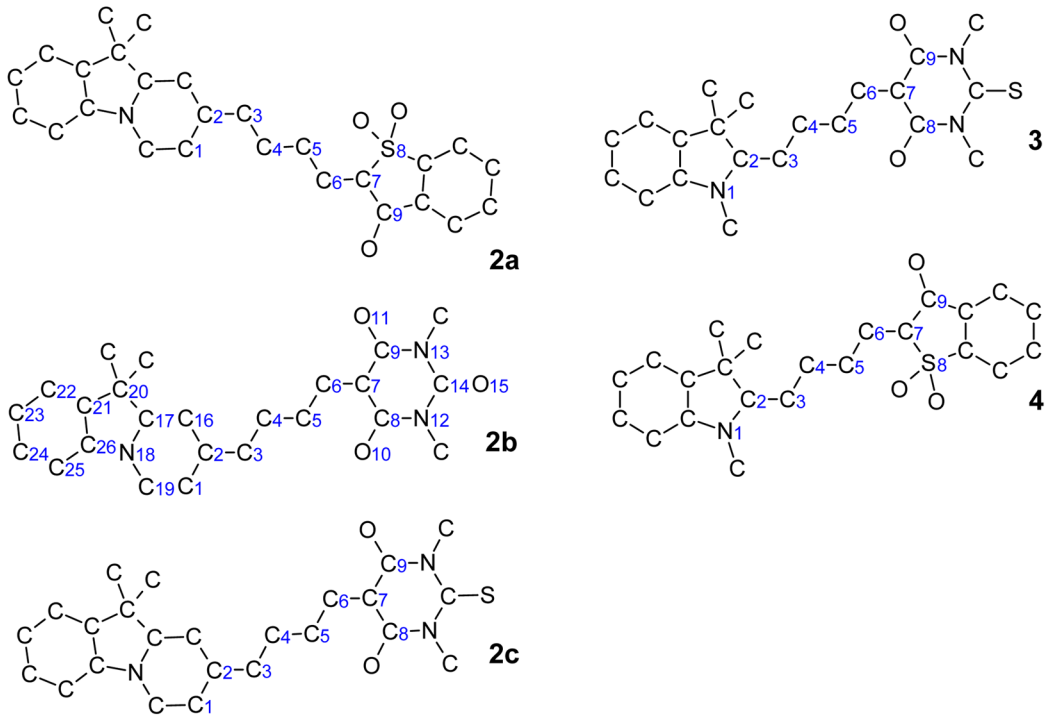

Chart 2.
Geometry-optimized structures and numbering convention for the merocyanine dyes.

NIH-PA Author Manuscript
NIH-PA Author Manuscript
NIH-PA Author Manuscript

NIH-PA Author Manuscript NIH-PA Author Manuscript NIH-PA Author Manuscript

Table 1

Calculated Relative Energies (kcal mol^{-1}) of the Different Isomers of Each Dye Molecule in C_6H_6 and MeOH.[a]

		Isomers			
		1 *trans* 4	**1 *cis* 4**	**1 *trans* 4**	**1 *cis* 4**
Dye	**Solvent**	**9 *trans* 5**	**9 *trans* 5**	**9 *cis* 5**	**9 *cis* 5**
I-TBA	C6H6	0.00	2.42		
	MeOH	0.00	2.45		
AI-TBA(4)	C6H6	0.00	0.38		
	MeOH	0.00	0.56		
AI-BA(4)	C6H6	0.00	1.72		
	MeOH	0.00	0.63		
I-SO	C6H6	0.05	0.66	0.00	1.66
	MeOH	0.00	0.80	0.43	1.95
AI-SO(4)	C6H6	0.56	0.00	1.72	1.08
	MeOH	0.75	0.00	2.04	2.03

[a]See structures in Chart 2 for the atomic labelling. Here for instance, “1 *trans* 4, 9 *trans* 5” means that “atom 1 is *trans* to atom 4, and atom 9 is *trans* to atom 5”.

NIH-PA Author Manuscript NIH-PA Author Manuscript NIH-PA Author Manuscript

Table 2

Observed Absorption Properties of Dyes 1a–b, 2a–d, 3, 4.

Solvent	3	4	2a,	2b,	2c,	2d,	1a,	1b,
	I-TBA	I-SO	AI-SO(4)	AI-BA(4)	AI-TBA(4)	P-SO(4)	P-SO(2)	AI-SO(2)
	λ_{max}/nm (ε)	λ_{max}/nm (ε^a)	λ_{max}/nm (ε)	λ_{max}/nm (ε)	λ_{max}/nm (ε)	λ_{max}/nm (ε)	λ_{max}/nm (ε)	λ_{max}/nm (ε)
MeOH	583 (173000)	586 (143000)	610 (65000)	585 (83000)	576 (38000)	580 (54000)	505 (57000)	542 (92000)
EtOH	-	-	636 (83000)	604 (104000)	603 (46000)	557 (61000)	514 (65000)	549 (111000)
i-PrOH	-	-	648 (122000)	614 (132000)	618 (50000)	597 (68000)	518 (72000)	553 (132000)
BuOH	589 (190000)	587 (134000)	650 (118000)	615 (154000)	619 (53000)	593 (64000)	519 (67000)	554 (120000)
OcOH	590 (180000)	587 (125000)	660 (150000)	628 (143000)	633 (97000)	612 (80000)	524 (72000)	559 (150000)
DMF	589 (183000)	586 (143000)	651 (154000)	625 (146000)	616 (52000)	604 (99000)	522 (92000)	556 (157000)
DMSO	-	-	644 (118000)	617 (122000)	607 (56000)	599 (77000)	520 (75000)	555 (126000)
CH_3CN	-	-	642 (142000)	621 (141000)	615 (54000)	596 (93000)	546 (89000)	549 (149000)
CH_2Cl_2	-	-	667 (278000)	647 (224000)	655 (104000)	629 (187000)	529 (128000)	561 (218000)
C_6H_6	584 (127000)	571 (109000)	679 (240000)	662 (201000)	683 (135000)	644 (178000)	538 (169000)	570 (235000)

J Phys Chem A. Author manuscript; available in PMC 2013 August 13.

NIH-PA Author Manuscript NIH-PA Author Manuscript NIH-PA Author Manuscript

Table 3

DFT Calculated Central C–C Bond Lengths (Å) of the Ground State Dye Molecules in C_6H_6 and in MeOH.

Solvent	Bond	Solute				
		I-TBA	AI-TBA(4)	AI-BA(4)	I-SO	AI-SO(4)
C_6H_6	C_2–C_3	1.394	1.413	1.411	1.386	1.412
	C_3–C_4	1.404	1.403	1.404	1.409	1.395
	C_4–C_5	1.393	1.403	1.401	1.383	1.394
	C_5–C_6	1.397	1.396	1.399	1.404	1.401
	C_6–C_7	1.402	1.408	1.404	1.382	1.386
BLA(C_6H_6) [a]		0.007	0.009	0.010	0.022	0.005
MeOH	C_2–C_3	1.401	1.430	1.427	1.398	1.429
	C_3–C_4	1.395	1.389	1.393	1.399	1.382
	C_4–C_5	1.402	1.419	1.416	1.396	1.410
	C_5–C_6	1.390	1.384	1.387	1.396	1.388
	C_6–C_7	1.415	1.426	1.421	1.395	1.404
BLA(MeOH) [a]		0.009	0.038	0.032	0.0005	0.035

[a] Bond length alternations, BLA = $\{|(C_2–C_3) – (C_3–C_4)| + |(C_4–C_5) – (C_5–C_6)|\}/2$

NIH-PA Author Manuscript NIH-PA Author Manuscript NIH-PA Author Manuscript

J Phys Chem A. Author manuscript; available in PMC 2013 August 13.

Table 4

SCRF/VSCRF Calculated and Experimentally (Exp) Observed Absorption (E_{abs}) Energies (eV), and the Relaxed S_0 State (μ_{S0}) and Vertical S_1 (μ^{v}_{S1}) State Dipole Moments (D) for the Dyes in C_6H_6 and in MeOH. TDDFT Calculated Absorption Energies (eV) for AI-BA(4) are Also Given Here.

Absorption						
				E_{abs}		
Solute	**Solvent**	μ_{S0}	μ^{v}_{S1}	**SCRF/VSCRF**	**TDDFT**	**Exp**
I-TBA	C_6H_6	16.53	17.86	1.611		2.123 (585 nm)
	MeOH	22.68	22.60	1.599		2.127 (583 nm)
AI-TBA(4)	C_6H_6	22.84	19.77	1.349		1.816 (683 nm)
	MeOH	32.54	25.19	1.581		2.153 (576 nm)
AI-BA(4)	C_6H_6	19.78	18.46	1.411	2.347	1.873 (662 nm)
	MeOH	28.60	21.60	1.583	2.373	2.120 (585 nm)
I-SO	C_6H_6	10.07	16.91	1.637		2.172 (571 nm)
	MeOH	14.64	17.63	1.556		2.116 (586 nm)
AI-SO(4)	C_6H_6	17.71	18.56	1.401		1.826 (679 nm)
	MeOH	26.16	23.83	1.536		2.120 (585 nm)

NIH-PA Author Manuscript

NIH-PA Author Manuscript

NIH-PA Author Manuscript

Table 5

Main Bond Lengths (Å) of the S_0 State AI-BA(4) Structure in MeOH with 0, 1, 2 and 3 Explicit H-Bonding CH_3OH Molecules.[a]

Bond	+0CH_3OH	+1CH_3OH(I)	+2CH_3OH(I,II)	+3CH_3OH(I,II,III)
C_2–C_3	1.427	1.435	1.443	1.444
C_3–C_4	1.393	1.382	1.381	1.380
C_4–C_5	1.416	1.414	1.418	1.418
C_5–C_6	1.387	1.385	1.384	1.383
C_6–C_7	1.421	1.420	1.424	1.425
C_7–C_8	1.451	1.445	1.442	1.441
C_7–C_9	1.450	1.445	1.447	1.444
C_1–C_{19}	1.369	1.373	1.373	1.373
C_{16}–C_{17}	1.371	1.385	1.390	1.390

[a]See atomic labels of AI-BA(4) in Chart 2, and the CH_3OH molecular positions of I, II, and III in Figure 7. Geometries were optimized using the COSMO model in ADF.

NIH-PA Author Manuscript NIH-PA Author Manuscript NIH-PA Author Manuscript

Table 6

SCRF/VSCRF and TDDFT Calculated Absorption (or Excitation) (E_{abs}) Energies (eV), the Relaxed S_0 State (μ_{S0}) and Vertical S_1 (μ^{V}_{S1}) State Dipole Moments (D) for AI-BA(4) in different H-bonding Models in MeOH (Figure 7), and the Absorption Energy Shifts from C_6H_6 to MeOH Solvents.

Absorption							
			E_{abs}		E_{abs}(MeOH) – E_{abs}(C_6H_6)[a]		
Model	μ_{S0}	μ^{V}_{S1}	SCRF/VSCRF	TDDFT	SCRF/VSCRF	TDDFT	Exp
+0CH_3OH	28.60	21.60	1.583	2.373	0.172	0.026	
+1CH_3OH	31.44	24.03	1.611	2.358	0.200	0.011	
+2CH_3OH	33.31	25.64	1.631	2.350	0.220	0.003	0.247
+3CH_3OH	34.63	26.89	1.648	2.353	0.237	0.006	

[a]The values of E_{abs}(MeOH) are the E_{abs} values given in the table for different models. $E_{abs}(C_6H_6)$ = 1.411 eV for VSCRF and 2.347 eV for TDDFT, which were given in Table 4.

J Phys Chem A. Author manuscript; available in PMC 2013 August 13.

NIH-PA Author Manuscript
NIH-PA Author Manuscript
NIH-PA Author Manuscript

Table 7

Observed Emission Properties of Dyes **1a, b**, **2a-d**, **3** and **4**.

Solvent	**3, I-TBA**	**4, I-SO**	**2a, AI-SO(4)**	**2b, AI-BA(4)**	**2d, P-SO(4)**	**1a, P-SO(2)**	**1b, AI-SO(2)**
	λ_{max}/nm (Φ^a)	**λ_{max}/nm (Φ)**	**λ_{max}/nm (Φ)**	**λ_{max}/nm (Φ)**	**λ_{max}/nm (Φ)**	**λ_{max}/nm (Φ)**	**λ_{max}/nm (Φ)**
MeOH	603 (0.26)	615 (0.08)	665 (0.54)	618 (0.52)	630 (0.018)	529 (0.005)	561 (0.05)
EtOH	-	-	671 (0.82)	651 (0.19)	634 (0.029)	533 (0.008)	563 (0.09)
i-PrOH	-	-	673 (0.96)	652 (0.22)	636 (0.049)	532 (0.014)	565 (0.13)
BuOH	609 (0.61)	618 (0.54)	675 (0.92)	654 (0.29)	640 (0.048)	535 (0.015)	567 (0.16)
OcOH	609 (0.99)	617 (0.98)	679 (0.88)	656 (0.64)	6443(0.082)	536 (0.024)	569 (0.21)
DMF	611 (0.94)	615 (0.97)	673 (~1.0)	658 (0.26)	635 (0.10)	534 (0.025)	567 (0.16)
DMSO	-	-	673 (~1.0)	657 (0.23)	636 (0.067)	535 (0.024)	567 (0.24)
CH_3CN	-	-	667 (0.75)	652 (0.05)	632 (0.067)	531 (0.011)	561 (0.06)
CH_2Cl_2	-	-	681 (0.54)	664 (0.03)	650 (0.082)	541 (0.01)	571 (0.06)
C_6H_6	605 (0.20)	603 (0.42)	691 (0.19)	670 (0.01)	656 (0.002)	546 (0.004)	577 (0.02)

J Phys Chem A. Author manuscript; available in PMC 2013 August 13.

NIH-PA Author Manuscript NIH-PA Author Manuscript NIH-PA Author Manuscript

Table 8

SCRF/VSCRF Calculated and Experimentally Observed Emission (E_{em}) Energies (eV), and the Relaxed S_1 State (μ_{S1}) and Vertical S_0 (μ^v_{S0}) State Dipole Moments (D) for the Dye Molecules in C_6H_6 and in MeOH.

Emission						
					E_{em}	
Solute	**Solvent**		**μ_{S1}**	**μ^v_{S0}**	**SCRF/VSCRF**	**Exp**
I-TBA	C_6H_6		18.21	17.00	1.506	2.050 (605 nm)
	MeOH		23.06	21.61	1.489	2.056 (603 nm)
AI-BA(4)	C_6H_6		17.27	20.07	1.341	1.851 (670 nm)
	MeOH	+0	19.23	23.91	1.416	2.006 (618 nm)
		+1	21.37	26.57	1.426	
		+2	23.17	28.26	1.428	
		+3	24.16	29.41	1.432	
I-SO	C_6H_6		16.85	10.55	1.629	2.056 (603 nm)
	MeOH		17.33	15.55	1.537	2.016 (615 nm)
AI-SO(4)	C_6H_6		18.57	18.15	1.332	1.794 (691 nm)
	MeOH		23.00	23.31	1.381	1.865 (665 nm)

NIH-PA Author Manuscript

NIH-PA Author Manuscript

NIH-PA Author Manuscript

Table 9

Calculated Central C–C Bond Lengths (Å) of the S_1 State Adiabetic Minimum Dye Molecules in C_6H_6 and in MeOH.

		Solute		
Solvent	**Bond**	**I-SO**	**AI-SO(4)**	**AI-BA(4)**
C_6H_6	C_2–C_3	1.400	1.430	1.431
	C_3–C_4	1.402	1.403	1.400
	C_4–C_5	1.408	1.412	1.419
	C_5–C_6	1.396	1.401	1.397
	C_6–C_7	1.405	1.398	1.415
MeOH	C_2–C_3	1.393	1.420	1.422
	C_3–C_4	1.414	1.416	1.413
	C_4–C_5	1.395	1.399	1.410
	C_5–C_6	1.410	1.414	1.405
	C_6–C_7	1.397	1.392	1.414

NIH-PA Author Manuscript

NIH-PA Author Manuscript

NIH-PA Author Manuscript

Table 10

Dyes Photobleaching Rates and Reactivity Towards Singlet Oxygen.

Dye	k_{ph}*106, s^{-1} (k_{ph}(rel))[a]		k_r(rel)[b]
	MeOH	C_6H_6	
2a, AI-SO(4)	89 (261)	128(115)	59.2
2b, AI-BA(4)	68 (200)		25.6
1a, P-SO(4)	28 (82)		60.3
2d, AI-SO(2)	0.7(2.1)		20.3
3, I-SO	0.53 (1.56)	1.11(1.00)	5.24
4, I-TBA	0.34 (1.00)		1.00
Cy5	1.89 (5.56)		

[a] k_{ph} = absolute rate of photobleaching, k_{ph}(rel) = relative rate of photobleaching with respect to standards I-TBA in MeOH and I-SO in C_6H_6.

[b] k_r(rel) = relative rates constants for product formation during reaction of the dyes with singlet oxygen produced chemically in DMSO. All measurements were done at 25 °C.

NIH-PA Author Manuscript

NIH-PA Author Manuscript

NIH-PA Author Manuscript

Table 11

Calculated Atomic Eletrostatic Potential (ESP) Charges of the Central C atoms of Ground State I-SO, AI-SO(4) and AI-BA(4) in MeOH.

Dyes	C_3	C_4	C_5	C_6
I-SO	−0.36	−0.10	−0.36	0.02
AI-SO(4)	−0.40	−0.11	−0.35	−0.02
AI-BA(4)	−0.47	−0.09	−0.32	−0.04

NIH-PA Author Manuscript

NIH-PA Author Manuscript

NIH-PA Author Manuscript

Table 12

Vertical Ionization Potential ΔE_I (eV) of I-SO, AI-SO(4) and AI-BA(4).

	Solute		
Solvent	**I-SO**	**AI-SO(4)**	**AI-BA(4)**
C_6H_6	6.083	5.953	5.908
MeOH	6.296	6.130	6.234